Quantitative evaluation of electromagnetic enhancement in surface-enhanced resonance Raman scattering from plasmonic properties and morphologies of individual Ag nanostructures

Ken-ichi Yoshida,[1,2] Tamitake Itoh,[1,*] Hiroharu Tamaru,[3] Vasudevanpillai Biju,[1] Mitsuru Ishikawa,[1] and Yukihiro Ozaki[2]
[1]*Nano-Bioanalysis Team, Health Technology Research Center, National Institute of Advanced Industrial Science and Technology (AIST), Takamatsu, Kagawa 761-0395, Japan*
[2]*Department of Chemistry, School of Science and Technology, Kwansei Gakuin University, Sanda, Hyogo 669-1337, Japan*
[3]*Photon Science Center, The University of Tokyo, Tokyo 113-8656, Japan*
(Received 28 May 2009; revised manuscript received 27 November 2009; published 3 March 2010)

The electromagnetic (EM) enhancement in surface-enhanced resonance Raman scattering (SERRS) is quantitatively evaluated for rhodamine molecules adsorbed on Ag nanostructures. Polarization dependence of the plasma resonance (plasmon resonance) and the SERRS spectra from single isolated Ag nanostructures was evaluated to determine one-to-one relationship between optical anisotropy of plasma resonance, that of SERRS, and the morphology of the nanostructures. Experimental observations were compared with finite-difference time-domain calculations of the EM field induced by plasma resonance using individual morphology of the nanostructures. The experimental enhancement factor of SERRS $\sim 10^9$ was consistent with that of the calculations within a factor of ~ 2 for three excitation wavelengths. We conclusively fortify the indispensible importance of SERRS-EM theory with our results to design metal nanostructures generating strong EM enhancement.

DOI: 10.1103/PhysRevB.81.115406 PACS number(s): 73.20.Mf, 03.50.De, 33.20.−t, 33.80.−b

I. INTRODUCTION

Nanostructures of Ag and Au generate strong enhancement of resonance Raman scattering of molecules adsorbed on their surfaces. This phenomenon is widely known as surface-enhanced resonance Raman scattering (SERRS). Enhancement factors of SERRS reach 10^{8-11} allowing us to detect single molecules (SMs).[1–4] Thus, SERRS is expected to be one of the ultrasensitive analysis methods. A theoretical model for the SM SERRS detection has been provided by SERRS electromagnetic (SERRS-EM) theory.[5–9] This theory predicts that the plasma resonance (plasmon resonance) (Ref. 10) in metal nanostructures, strongly coupling with the incident and the scattered light, also enhances the electromagnetic coupling for the Raman scattering of the molecule.[5–9] Thus, experimental verification of the relationship between the plasma resonance, the EM enhancement of SERRS, and the morphology of the metal nanostructures observed are of crucial importance for demonstration of the reliability of the SERRS-EM theory.[5–9]

Because plasma resonance in metal nanostructures is highly sensitive to the subtle difference in their shape and size, their morphologies affect strongly SERRS enhancement under the SERRS-EM model.[4–22] Ensemble measurement averages over spectra of plasma resonance and SERRS of individual Ag nanostructures. Indeed, the ensemble measurement obscures the plasma resonance inducing SERRS and the morphology of Ag nanostructures that determines the plasma resonance. To lift the issue of the obscurity, we have observed plasma resonance and SERRS spectra from single isolated Ag nanostructures by dark-field microspectroscopy and identified the plasma resonance inducing SERRS-EM enhancement.[19–22] This identification enabled us to reveal that spectral shapes of SERRS-EM enhancement factors are equivalent to those of the plasma resonance. However, the enhancement factor was only a fitting parameter to reproduce experimental observations in the previous study.[22] The enhancement factor thus determined is consistent with the morphology of single Ag nanostructures assumed to be a dimer of Ag nanoparticles.[22] Thus, we have demonstrated the validity of the SERRS-EM theory under such assumption. However, without the morphology of Ag nanostructures, we cannot rigorously calculate the plasma resonance, SERRS-EM enhancement factors, and SERRS spectra of isolated Ag nanostructures.[18,23,24]

In the current study, we observed the morphology of single isolated Ag nanostructures using scanning electron microscopy (SEM) to decide the issue of *assumed* SERRS enhancement factors. The morphology of Ag nanostructures was used to define the boundary for EM calculation of the plasma resonance using finite-difference time-domain (FDTD) method.[25] First of all, we roughly calculated EM enhancement factors with mesh size of 1.5 nm. The calculated EM factors totally failed to reproduce experimental ones. We thus examined further EM enhancement factors of Ag nanostructures using smaller mesh size to improve the accuracy in the calculations. The use of 0.2 nm mesh size allowed us to obtain quantitatively acceptable FDTD calculations of EM enhancement factors. On the other hand, the use of 1.5 nm mesh size in the FDTD calculations quantitatively reproduced plasma-resonance spectra themselves due to the long distance (>100 nm) between calculation points for plasma resonance and an Ag surface. Multiplying the calculated EM enhancement factors by experimental resonance Raman spectra quantitatively reproduced experimental SERRS spectra. Furthermore, excitation wavelength dependence of SERRS spectra confirmed the quantitative reproduction of SERRS spectra.

II. EXPERIMENT

A suspension of Ag colloids was prepared following the method of Lee and Meisel.[26] A NaCl aqueous solution (25

mM) of Rhodamine 6G (R6G, $\sim 10^{-8}$ M) was mixed with the Ag colloidal suspension (7.2×10^{-11} M). After incubating the mixture at room temperature (~ 20 °C) for 15 min, it was spin coated on a glass plate covered with a 60-nm-thick indium tin oxide (ITO) film. This initial concentration of R6G is substantially higher than the standard recipe for single-molecule SERRS experiments ($\sim 10^{-11}$ M) but was unavoidable to provide sufficient number of Ag nanostructures showing SERRS activity. However, the effective concentration of R6G was reduced by rinsing away most of the R6G molecules adsorbed on both Ag nanostructures and the glass surface using acetone and water.[20,22] The spectral shape and intensity of both SERRS and the background signal from the resulting samples were quantitatively comparable to those prepared with $\sim 10^{-11}$ M R6G, and fluorescence signals were never detected from the glass surface. With these results, we are safe to assume the effective concentrations of the dye in our experiments to be equivalent to those for SM SERRS.

The detail of our spectroscopic setup is described elsewhere[19] but is briefly described as follows: white light from a 50 W halogen lamp was focused with a dark-field condenser lens to acquire the Rayleigh scattering spectra from the structures. Rayleigh scattering is, in principle, due to plasma resonances in metal nanostructures. The spectra due to Rayleigh scattering are therefore referred to as plasma-resonance spectra hereafter. A frequency-doubled YAG laser (532 nm, 2 W/cm^2), a yellow DPSS laser (561 nm, 2 W/cm^2), and a He-Ne laser (633 nm, 2 W/cm^2) were used as the sources for acquiring the SERRS spectra. Both of these spectra were acquired for single isolated Ag nanostructures dispersed on an ITO glass plate by means of dark-field microspectroscopy. The spectra of SERRS and plasma-resonance-scattering intensities (photocounts) were converted into the cross-section spectra of SERRS (cm^2) and those of plasma-resonance scattering (cm^2) using 80 nm gold nanosphere, whose scattering intensity and scattering cross section are known. Note that the conversion factor for SERRS is 2.3×10^{-18} (cm^2/photocounts) and the conversion factor for plasma-resonance scattering is 2.3×10^{-18} (cm^2/photocounts) on the current spectroscopic equipment.

After the spectroscopic measurements, the whole sample, including the ITO glass plate, was sent to a SEM (JSM-6700F, JEOL) for the identification of the morphologies of the nanostructures.[16,23,24] The shapes, sizes, and orientations of the nanostructures that were read off the acquired SEM images were used to model the structures for the FDTD calculation that is used to evaluate the local intensities of the EM field. Ideally, the substrate should also be modeled within the FDTD calculation but for simplicity, we chose an effective refractive index that homogeneously surrounds the nanostructures as $n_{\mathrm{env}}=1.3$. This value is reasonable for the nanostructures on an ITO glass plate ($n \sim 1.8$) and measured in air ($n \sim 1.0$).[27–30]

III. RESULTS AND DISCUSSION

The spectrum of SERRS-EM enhancement factor $M_{\mathrm{EM}}(\lambda_{\mathrm{L}},\lambda,\boldsymbol{r})$ is written as a product of first and second enhancement factors, each of which is induced by coupling of plasma resonance with incident light and resonance Raman-scattered light.[5–7,31] Thus, $M_{\mathrm{EM}}(\lambda_{\mathrm{L}},\lambda,\boldsymbol{r})$ is given by

$$M_{\mathrm{EM}}(\lambda_{\mathrm{L}},\lambda,\boldsymbol{r}) = M_1(\lambda_{\mathrm{L}},\boldsymbol{r})M_2(\lambda,\boldsymbol{r}) = \left|\frac{E^{loc}(\lambda_{\mathrm{L}},\boldsymbol{r})}{E^{I}(\lambda_{\mathrm{L}})}\right|^2 \times \left|\frac{E^{loc}(\lambda,\boldsymbol{r})}{E^{I}(\lambda)}\right|^2, \quad (1)$$

where E^I and E^{loc} indicate the amplitudes of the incident and the local electric field, respectively; λ_{L} and λ denote the wavelengths of incident and Raman-scattering light, respectively; $\boldsymbol{r}$ is an arbitrary position; and M_1 and M_2 are the enhancement factors of excitation and scattered light, respectively. To obtain the total SERRS enhancement factor, $M_{\mathrm{EM}}(\lambda_{\mathrm{L}},\lambda,\boldsymbol{r})$ in Eq. (1) is summed over the location of dye molecules on the Ag nanostructure, and is thus rewritten as[32]

$$M_{\mathrm{EM}}^{\mathrm{Total}}(\lambda_{\mathrm{L}},\lambda) = \sum_{i=1}^{N} M_1^i(\lambda_{\mathrm{L}},\boldsymbol{r}_i)M_2^i(\lambda,\boldsymbol{r}_i), \quad (2)$$

where M_1^i and M_2^i are the enhancement factors of excitation and scattered light at the the center of gravity ($\boldsymbol{r}_i$) of a molecule i, and N is the total number of molecules.

Accordingly, the SERRS cross-section spectra $\sigma_{\mathrm{S}}(\lambda_{\mathrm{L}},\lambda)$ is given by[5]

$$\sigma_{\mathrm{S}}(\lambda_{\mathrm{L}},\lambda) = \sum_{i=1}^{N} \sigma_{\mathrm{R}}(\lambda_{\mathrm{L}},\lambda)M_1^i(\lambda_{\mathrm{L}},\boldsymbol{r}_i)M_2^i(\lambda,\boldsymbol{r}_i), \quad (3)$$

where σ_{R} $(\lambda_{\mathrm{L}},\lambda)$ is the resonance Raman-scattering cross-section spectrum of the molecule without surface enhancement. For an Ag dimer, the largest EM field inducing SM SERRS is generated only at the crevice of Ag nanostructures,[14,15] and this largest EM field at the crevice dominates the value of $M_{\mathrm{EM}}^{\mathrm{Total}}(\lambda_{\mathrm{L}},\lambda)$.[14,15] Thus, $\Sigma_{i=1}^{N} M_1^i(\lambda_{\mathrm{L}},\boldsymbol{r}_i)M_2^i(\lambda,\boldsymbol{r}_i)$, is approximately written as $M_1(\lambda_{\mathrm{L}},\boldsymbol{r_o})M_2(\lambda,\boldsymbol{r_o})$ for a single molecule in the crevice even if some additional molecules exist at positions other than the crevice. Here, $\boldsymbol{r_o}$ denotes the position at the crevice, examples of which are shown in Figs. 6(i), 7(h), and 9(k). In short, we assume that $M_{\mathrm{EM}}^{\mathrm{Total}}(\lambda_{\mathrm{L}},\lambda)=M_1(\lambda_{\mathrm{L}},\boldsymbol{r_o})M_2(\lambda,\boldsymbol{r_o})$ for the evaluation of our experimental SERRS enhancement factors. Note that $M_1(\lambda_{\mathrm{L}},\boldsymbol{r_o})M_2(\lambda,\boldsymbol{r_o})$ is further simplified to $M_1(\lambda_{\mathrm{L}},\boldsymbol{r_o})^2$ assuming λ_{L} close to λ.

To calculate $\sigma_{\mathrm{S}}(\lambda_{\mathrm{L}},\lambda)$ in Eq. (3), we need $\sigma_{\mathrm{R}}(\lambda_{\mathrm{L}},\lambda)$ of R6G molecules. However, we cannot easily measure $\sigma_{\mathrm{R}}(\lambda_{\mathrm{L}},\lambda)$ of R6G because strong fluorescence disturbs us to detect resonance Raman-scattering light. The resonance Raman-scattering spectrum of R6G has been measured by removing strong fluorescence using an ultrafast Kerr shutter.[33] However, such measurements provided resonance Raman-scattering spectra with low-energy resolution whose spectral resolution does not meet the current requirement for calculation. To resolve the issue of the low resolution, we substitute $\sigma_{\mathrm{S}}(\lambda_{\mathrm{L}},\lambda)$ of an ensemble of Ag nanoaggregates adsorbed by R6G for $\sigma_{\mathrm{R}}(\lambda_{\mathrm{L}},\lambda)$, assuming that spectral shape of $\sigma_{\mathrm{R}}(\lambda_{\mathrm{L}},\lambda)$ is equivalent to that of $\sigma_{\mathrm{S}}(\lambda_{\mathrm{L}},\lambda)$ evaluated from the ensemble. We described the rationale behind this assumption.[21,22] The key to this assumption is that a spectral shape of plasma resonance of the ensemble Ag nanoaggre-

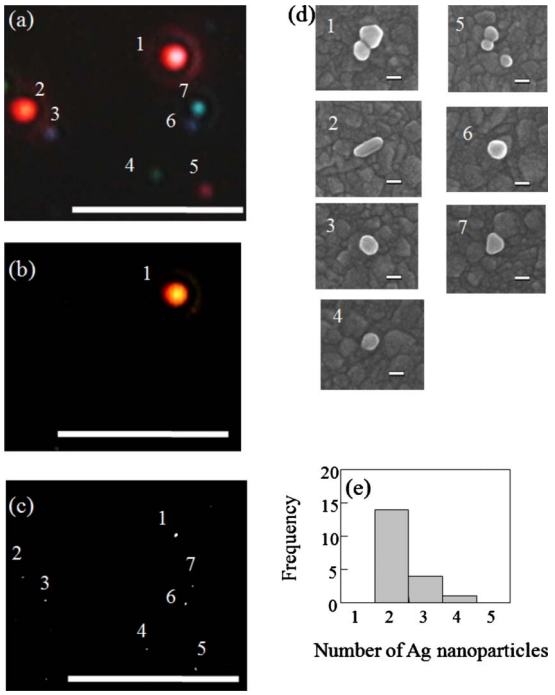

FIG. 1. (Color online) Images of (a) Rayleigh scattering due to plasma resonance, (b) SERRS, and (c) SEM obtained from the same area on a sample glass plate covered with an indium tin oxide (ITO) film. (d) Enlarged SEM images of Ag nanostructures numbered in (a)–(c). SERRS images of the particles numbered from 1 to 7 were observed by circularly polarized 532 nm excitation. (e) Histogram of the number of Ag nanoparticles included in SERRS-active nanostructures. The histogram was obtained from 19 Ag nanostructures screened by the measurement of SEM images, Rayleigh scattering images, and SERRS spectra. In short, we empirically selected Ag nanostructures showing well-defined appearance, Rayleigh scattering in narrowband color, and SERRS activity. Scale bars in (a)–(c) and (d) are 5 μm and 50 nm, respectively.

gate is almost flat (data not shown) in the 500–750 nm region due to randomly overlapped plasma resonance, spectral maxima of which are different from Ag aggregate to aggregate. The SERRS-EM theory predicts that spectral shape of plasma-resonance spectra are similar to that of $M_1(\lambda_L)M_2(\lambda)$ spectra.[5,6] Thus, the spectral shape of $M_1(\lambda_L)M_2(\lambda)$ will be also flat for the ensemble Ag nanoaggregate. The flat shape of $M_1(\lambda_L)M_2(\lambda)$ assures that each Raman spectral line is uniformly enhanced. The uniform enhancement makes the SERRS spectrum of an ensemble of Ag nanoaggregates similar to the conventional resonance Raman spectrum. Indeed, the SERRS spectrum of an ensemble Ag nanoaggregate is quite similar to the resonance Raman spectrum.[33] Note that we determined the magnitude of $\sigma_R(\lambda_L,\lambda)$ (cm^2) itself using a Raman-scattering cross section of R6G estimated by Fermi's golden rule.[6]

Figures 1(a)–1(c) show a set of images of plasma resonance, SERRS, and SEM acquired from the same area of a sample on the ITO glass plate. These images identify single isolated Ag nanostructures that correlate plasma resonance, SERRS, and morphologies of the Ag nanostructures. The spots from plasma resonance in Fig. 1(a) are attributed to the dipolar or the first TM mode of the plasma resonance from narrowband colors such as red (in print; light gray color), green (in print; dark gray color), and blue (in print; gray color).[19–24,34] Figure 1(d) shows the magnified SEM images of Ag nanoparticles numbered in Figs. 1(a)–1(c). The Ag nanostructures showing narrowband colors have simple morphology such as monomer, dimer, or trimer. In the current work, we selected Ag nanostructures showing both well-defined plasma resonance and SERRS activity, and measured their spectra and morphologies in one-to-one correspondence. Figure 1(e) shows a histogram of the number of Ag nanoparticles that forms the nanostructure fulfilling such selection criteria, and they have the tendency to favor dimers. A dimer is the simplest structure generating highly enhanced SERRS.[4,18,23] The morphology of Ag nanostructure observed by SEM was used for modeling the structure for FDTD calculation.

We compare the experimental results with the FDTD calculations of a monomer, a dimer, a trimer, and a tetramer composed of Ag nanoparticle(s). In general, FDTD calculation causes a problem about quantitative evaluation of $M_1(\lambda_L,\boldsymbol{r})$ at surfaces with large curvature such as nanopaticles because a nanoparticle is treated as an ensemble of cubic cells within the Yee algorism, i.e., the smooth curved surface of a nanoparticle is approximated by stair-cased surfaces.[25] Thus, evaluation of absolute $M_1(\lambda_L,\boldsymbol{r})$ as much as possible is time consuming to do. For this reason, we first of all carried out FDTD calculation using a mesh size 1.5 nm to find spatial distribution of $M_1(\lambda_L,\boldsymbol{r})$ on an Ag nanoparticle. Here we compare the calculations using 1.5 nm mesh with experimental observations. Figures 2(a)–2(c), 3(a)–3(c), 4(a)–4(c), and 5(a)–5(c) show experimental SEM images, plasma-resonance spectra, and SERRS spectra obtained from the identical Ag monomer, dimer, trimer, and tetramer, respectively. Figures 2(d)–2(f), 3(d)–3(f), 4(d)–4(f), and 5(d)–5(f) show the boundary conditions for the FDTD calculation, calculated plasma-resonance spectra, and a calculated spatial distribution of $M_1(\lambda_L,\boldsymbol{r})$, respectively. The SEM images established the boundary conditions for the FDTD calculation. Excitation light is a circularly polarized 532 nm laser beam. The use of 1.5 nm mesh allows the experimental plasma-resonance spectra to be comparable in its spectral shape and cross section to the calculations for all the structures. For a monomer [Fig. 2(a)], we confirmed that the experimental plasma resonance, whose spectral maximum locates at 500 nm, assumes a dipolar character from dependence of its intensity on the polarization of excitation light (data not shown). The calculated spatial distribution of EM field and its dependence on the polarization of excitation light also evidenced a dipolar nature of the plasma resonance (data not shown). For a dimer [Fig. 3(a)], we confirmed that both the experimental and the calculated plasma-resonance band at 630 nm are dipolar from the excitation polarization dependence [see Figs. 6(b) and 6(f)]. Similarly, we confirmed that both the experimental and the calculated plasma-resonance bands at 600 and 550 nm are generated by two different dipoles for a trimer [Fig. 4(a)] (data not shown) and that both the experimental and the calculated plasma-resonance bands at 690 and 550 nm are dipolar and quadripolar, respectively, for a tetramer [Fig. 4(a)] (data not shown). We consider that the quantitative reproduction of plasma-resonance spectra by

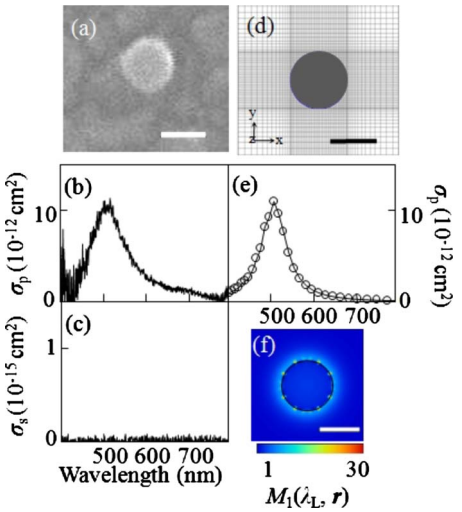

FIG. 2. (Color online) (a) SEM image, (b) experimental plasma-resonance spectrum, (c) experimental SERRS spectrum, (d) modeled structure of the SEM image in the FDTD calculation, (e) calculated plasma-resonance spectra, and (f) calculated spatial distribution of EM enhancement factors of an Ag monomer. Note that the structure for the FDTD calculation in (d) was determined from the experimental SEM image in (a). Experimental plasma-resonance maximum of an Ag monomer in (b) was observed at 500 nm; its full width at half maximum (FWHM) was ~100 nm and its cross section was $\sim 1 \times 10^{-11}$ cm^2. Mesh size 1.5 nm, refractive index 1.3 of the surrounding medium, and circularly polarized incident light (532 nm) were selected for the FDTD calculation. Scale bar in each panel is 50 nm.

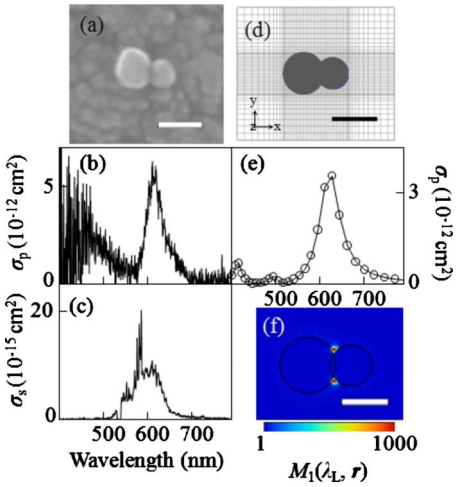

FIG. 3. (Color online) (a) SEM image, (b) experimental plasma-resonance spectrum, (c) experimental SERRS spectrum, (d) modeled structure of the SEM image in the FDTD calculation, (e) calculated plasma-resonance spectra, and (f) calculated spatial distribution of EM enhancement factors of an Ag dimer. Note that the structure for the FDTD calculation in (d) was determined from the experimental SEM image in (a). Experimental plasma-resonance maximum of an Ag dimer in (b) was observed at 615 nm; its FWHM was ~50 nm and its cross section was ~5 $\times 10^{-12}$ cm^2. Mesh size 1.5 nm, refractive index 1.3 of the surrounding medium, and circularly polarized incident light (532 nm) were selected for the FDTD calculation. Scale bar in each panel is 50 nm.

the FDTD calculations using 1.5 nm meshes is due to the enough long distance (>100 nm) between calculation points of surface integration for cross section and an Ag surface.[16,17]

The Ag nanostructures will define both plasma resonance and spatial distribution of $M_1(\lambda_L, \boldsymbol{r})$. Thus, the consistency between calculated and experimental plasma-resonance spectra for the identical Ag nanostructures makes it possible to expect that the calculated spatial distribution of $M_1(\lambda_L, \boldsymbol{r})$s also well approximate spatial distribution of $M_1(\lambda_L, \boldsymbol{r})$s around Ag nanostructures. For monomers without SERRS activity, no highly localized spots with large $M_1(\lambda_L, \boldsymbol{r})$ are found on the surface as shown in Fig. 2(f). On the other hand, for the dimer, the trimer, and the tetramer with SERRS activity, local spots with large $M_1(\lambda_L, \boldsymbol{r})$s are clearly observed around the Ag nanoparticle crevices as shown in Figs. 3(f), 4(f), and 5(f). The correlation between presence of SERRS activity and local spots with large $M_1(\lambda_L, \boldsymbol{r})$ has already been studied.[5,6] The current comparison between structure of Ag nanoparticles (experiments), plasma-resonance spectra (experiments and calculations), spatial distribution of $M_1(\lambda_L, \boldsymbol{r})$ (calculations), and SERRS activity (experiments) strongly supports the previous studies,[14,15] showing that SERRS signals are detected from local spots with large $M_1(\lambda_L, \boldsymbol{r})$s, i.e., "hot spots" in the SERRS-EM theory.

Under the current experimental conditions, we have identified that most of Ag nanostructures showing both dipolar plasma resonance and SERRS activity are dimers, as shown in Fig. 1(e). Theoretical studies have predicted that structural anisotropy of Ag dimers induces anisotropy in both plasma resonance and SERRS.[35,36] To verify the prediction, we measured anisotropy of both plasma-resonance and SERRS spectra, and then compared them with FDTD calculations of plasma-resonance spectra and $M_1(\lambda_L, \boldsymbol{r})$ using a mesh size 1.5 nm. The incidence light for the experiments and the calculations was linearly polarized with $\lambda_L = 532$ nm. Note that we estimated experimental $M_1(\lambda_L, \boldsymbol{r})$ from the square root of experimental $M_{EM}^{Total}(\lambda_L, \lambda) \sim M_1(\lambda_L, \boldsymbol{r_o})^2$. Figures 6(a)–6(c) show that the SEM image, the plasma-resonance spectra, and the SERRS spectra obtained from the identical Ag dimer. Figures 6(b) and 6(c) show that both the intensity of plasma-resonance maximum at 620 nm and that of SERRS maximum achieved the highest intensity at the polarization angle parallel to the dimer long axis. Figure 6(f) shows that the FDTD calculations of polarization dependence of a plasma-resonance spectrum of the Ag dimer in Fig. 6(e) well reproduced the experimental polarization dependence in Fig. 6(b). Figures 6(f) and 6(g) show that structural anisotropy of an Ag-dimer-induced splitting of plasma resonance into the longitudinal at 620 nm and transverse (<400 nm) mode, and coupling of the longitudinal plasma resonance with the light polarized along the long axis of an Ag dimer generated the largest $M_1(\lambda_L, \boldsymbol{r})$ at the dimer crevices. The agreement in experimental and calculated polarization dependence in Figs. 6(b) and 6(f) suggests that the calculated spatial distribution of $M_1(\lambda_L, \boldsymbol{r})$ in Fig. 6(g) reflects local EM fields around an Ag dimer. Thus, the SERRS in Fig. 6(c) is generated by EM fields coupled with the longitudinal plasma resonance at

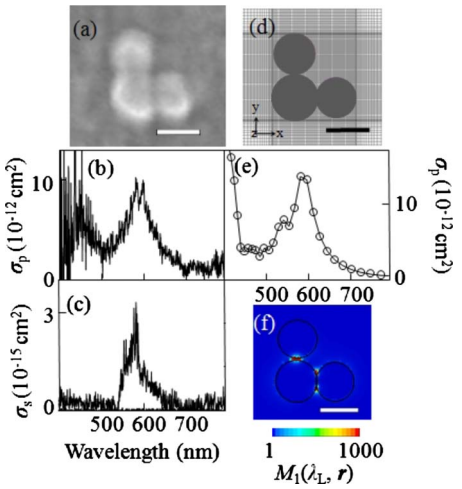

FIG. 4. (Color online) (a) SEM images, (b) experimental plasma-resonance spectrum, (c) experimental SERRS spectrum, (d) modeled structure of the SEM image in the FDTD calculation, (e) calculated plasma-resonance spectra, and (f) calculated spatial distribution of EM enhancement factors of an Ag trimer. Note that the structure for the FDTD calculation in (d) was determined from the experimental SEM image in (a). Experimental plasma-resonance maximum of a trimer in (b) was observed at 580 nm; its FWHM was ~90 nm and its cross section was $\sim 1 \times 10^{-11}$ cm^2. Mesh size 1.5 nm, refractive index 1.3 of the surrounding medium, and circularly polarized incident light (532 nm) were selected for the FDTD calculation. Scale bar in each panel is 50 nm.

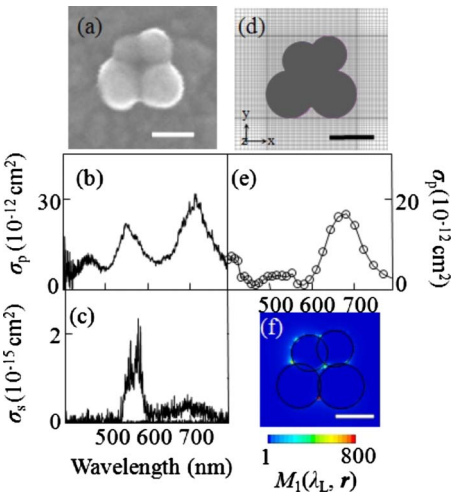

FIG. 5. (Color online) (a) SEM images, (b) experimental plasma-resonance spectra, (c) experimental SERRS spectra obtained from an Ag tetramer, (d) modeled structure of the SEM image in the FDTD calculation, (e) calculated plasma-resonance spectra, and (f) calculated spatial distribution of EM enhancement factors of an Ag tetramer. Note that the structure for the FDTD calculation in (d) was determined from the experimental SEM image in (a). Experimental plasma-resonance maxima of tetramer in (b) were observed at 700 and 550 nm; their FWHM were ~90 and ~80 nm, and their cross sections were $\sim 3 \times 10^{-11}$ cm^2 and 2×10^{-11} cm^2, respectively. Mesh size 1.5 nm, refractive index 1.3 of the surrounding medium, and circularly polarized incident light (532 nm) were selected for the FDTD calculation. Scale bar in each panel is 50 nm.

crevices. Indeed, Figs. 6(d) and 6(h) show that experimental anisotropy of plasma resonance and $M_1(\lambda_L, \boldsymbol{r})$ well agreed with the calculated anisotropy. Note that $\boldsymbol{r}$ was selected at an arbitrary position in the crevice in Fig. 6(i), as shown in the cross in Fig. 6(i). The agreement is consistent with the prediction by the SERRS-EM theory that anisotropy of Ag structures causes anisotropy of plasma resonance and SERRS. Additionally, we also confirmed the agreement between a structural anisotropy and an optical anisotropy for trimers (data not shown).

Until now, we have evaluated only $M_1(\lambda_L, \boldsymbol{r})$; however, we also must consider the other enhancement factor $M_2(\lambda, \boldsymbol{r})$ to evaluate the total spectral shape of EM field induced by plasma resonance. We thus examined relationship between experimental plasma-resonance spectra and spectra of $M_{EM}(\lambda_L, \lambda, \boldsymbol{r})$s including $M_2(\lambda, \boldsymbol{r})$ and calculated a spectral shape of $M_{EM}(\lambda_L, \lambda, \boldsymbol{r})$ of an Ag dimer. Figures 7(a)–7(c) show a SEM image of an Ag dimer, an experimental plasma-resonance spectrum, and an experimental SERRS spectrum, respectively. Figures 7(d)–7(f) show the boundary condition for an Ag dimer in the FDTD calculation, a calculated plasma-resonance spectrum, and a spectrum of $M_{EM}(\lambda_L, \lambda, \boldsymbol{r})$, respectively. The cross in Fig. 7(h) indicates the position $\boldsymbol{r}$ selected for the calculation of the spectrum in Fig. 7(f). Note that we selected $\boldsymbol{r}$ at an arbitrary position in the crevice in Fig. 7(h) simply because we do not consider rigorously the absolute value of $M_{EM}(\lambda_L, \lambda, \boldsymbol{r})$ in the calculations in Figs. 7(e)–7(g). Figures 7(b) and 7(e) show that the experimental plasma-resonance spectrum well agreed with the calculation. The agreement makes confident that the use of the SEM morphology is valid for the boundary condition in the FDTD calculation. Figures 7(e) and 7(f) show that the spectral shape of the plasma resonance was quite similar to that of $M_{EM}(\lambda_L, \lambda, \boldsymbol{r})$. The similarity is reasonable considering that the EM enhancement is induced by the plasma resonance.[21,22] Figure 7(c) shows that the SERRS spectrum around 610 nm was selectively enhanced by the plasma resonance in Fig. 7(b). We found that the selectively enhanced SERRS spectra are common all our experimental results in Figs. 3–7 and 9 and our previous reports.[21,22]

To quantitatively evaluate SERRS-EM enhancement factors using the conventional FDTD calculation with Yee cells, in which every components of an electric and a magnetic field are set at the center of a side and of a plane in a cubic cell,[25] we examined accuracy in our calculations by comparing FDTD calculations with self-consistent calculation under the common calculation conditions.[32] Note that we did not employ self-consistent calculation in the current work because the calculation is limited to asymmetrical Ag nanostructures[25] although it offers an exact solution of SERRS-EM enhancement factors for symmetrical Ag nanostructures, such as spheres, columns, and symmetric dimers.[32] We further address a problem about the use of Yee cells in FDTD calculation. The intensity of EM field is maximized at a surface and exponentially decays with increasing distance outside from the surface. However, for a surface having a curvature comparable to mesh size, the calculated exponential decay and the peak intensity of EM field will be

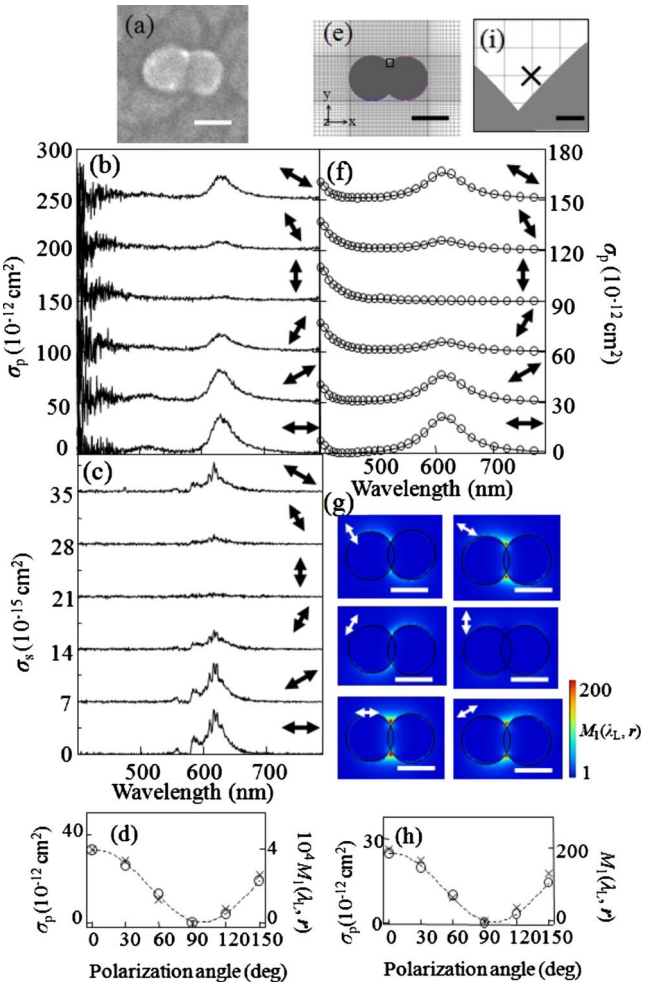

FIG. 6. (Color online) (a) SEM image, (b) polarization dependence of experimental plasma-resonance spectra, and (c) polarization dependence of experimental SERRS spectra of an Ag dimer. (d) Polarization-angle dependence of cross sections of experimental plasma resonance (open circles with a dashed curve) and experimental EM enhancement factors (crosses with a dashed curve). (e) Modeled structure of an Ag dimer for the FDTD calculation, (f) polarization dependence of a calculated plasma-resonance spectrum, and (g) polarization dependence of calculated spatial distribution of EM enhancement factors. (h) Polarization-angle dependence of cross sections of calculated plasma resonance (open circles with a dashed curve) and calculated EM factors (crosses with a dashed curve) as a function of polarization angles. (i) Magnified view in the vicinity of the crevice of the Ag dimer in (e). Scale bars in (a), (e), (g), and (i) are 50 nm, 50 nm, 50 nm and 1.5 nm, respectively. Mesh size 1.5 nm, refractive index 1.3 of the surrounding medium, and circularly polarized incident light (532 nm) were selected in the FDTD calculation.

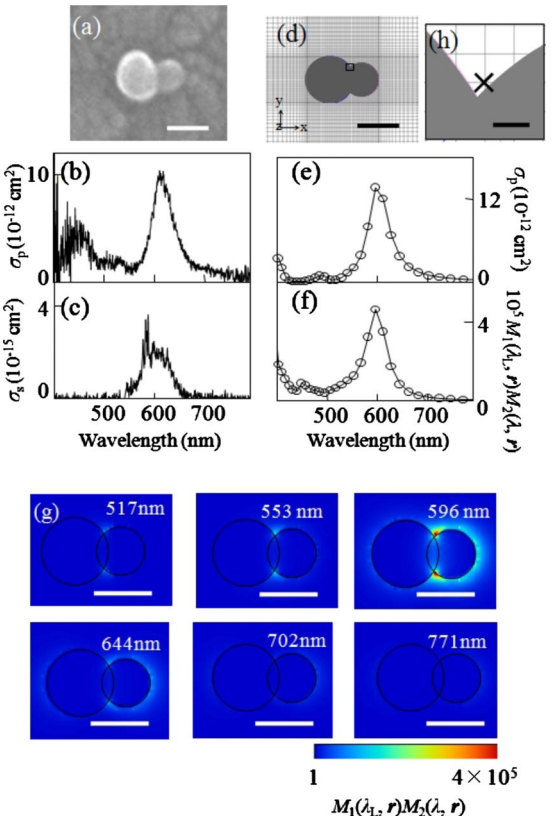

FIG. 7. (Color online) (a) SEM image, (b) experimental plasma-resonance spectrum, (c) experimental SERRS spectrum, (d) modeled structure in the FDTD calculation, (e) calculated plasma-resonance spectrum, and (f) calculated spectrum of EM enhancement factor of an Ag dimer. (g) Calculated spectrum of spatial distribution of SERRS-EM enhancement factors. (h) Magnified view in the vicinity of the crevice of the Ag dimer in (d). The SEM image, the plasma-resonance spectrum, and the SERRS spectrum in (a)–(c) were observed from the identical Ag nanoparticle. Spectrum of SERRS-EM enhancement factors in (f) was calculated at the position of cross in (h). Scale bars in (a), (d), (g), and (h) are 50 nm, 50 nm and 1.5 nm, respectively. Mesh size 1.5 nm, refractive index 1.3 of the surrounding medium, and circularly polarized incident light (532 nm) were selected in the FDTD calculation.

smoothed and smaller than the "real" intensity. In other words, the problem of FDTD calculation is averaging over EM fields at the surface. The problem results in underestimation of EM field intensity at the surface, and is not negligible for the surface having small curvature.[32] Fortunately, a factor of underestimation can be reduced by the use of smaller meshes. We selected the morphology of an Ag dimer equivalent to that in Fig. 2(a) of Ref. 32, and evaluated a factor of underestimation for the dimer with mesh size of 0.98, 0.5, and 0.2 nm; these values are smaller than the gap of the dimer. Figure 8(a) shows the morphology of the selected Ag dimer. The x axis is set to overlap with the long axis of the dimer. An EM field reaches the theoretical maximum at the local face-to-face surfaces along the x axis, as shown in the square in Fig. 8(a). Note that we used electric flux density instead of an EM field to avoid discontinuity of the field across the surface. Figure 8(b) shows the magnified view of the square in Fig. 8(a). Figure 8(c) shows a spectrum of $M_1(\lambda,\boldsymbol{r})^2$ calculated by the use of mesh size 0.98 nm. The spectral maximum locates at ~418 nm, which agrees with Fig. 2(a) in Ref. 32. This agreement provides evidence that the plasma resonance for the current FDTD calculation of $M_1(\lambda,\boldsymbol{r})^2$ is common to that in Ref. 32.

Here, we explain the criterion for the accuracy in the calculation of $M_1(\lambda,\boldsymbol{r})^2$. The distance d outside from the surface, where the electric flux density is reduced by a factor of

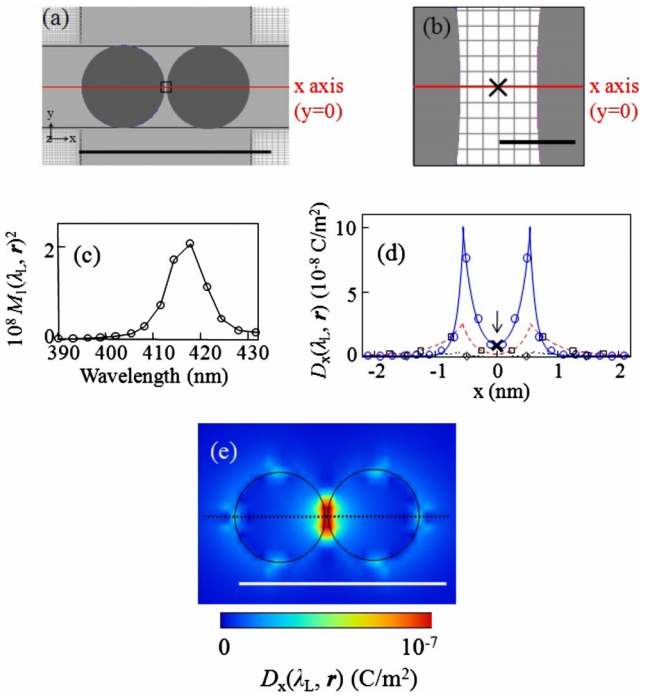

FIG. 8. (Color online) (a) Modeled structure of an Ag dimer in the FDTD calculation. (b) Magnified view of the vicinity of the gap in the modeled structure. (c) Calculation spectrum of the SERRS-EM enhancement factor at the cross in (b). (d) Calculation cross section of spatial distribution of the electric flux density (black dotted line, red broken line, and blue solid line; mesh size is 1.5 nm, 0.5 nm, and 0.2 nm, respectively). (e) Spatial distribution of the electric flux density D_x. The cross pointed by the arrow in (d) indicates the calculated enhancement factor in Fig. 2(a) of Ref. 32. Note that the cross section in (d) indicates the electric flux density along the dashed line in (e). Scale bars in (a), (b), and (e) is 50 nm, 1.0 nm, and 50 nm, respectively.

$|1/e|^2$, is defined as $d=N/(c\lambda)\sqrt{-\varepsilon(\lambda)}$. Here n is refractive index of bulk Ag (or a vacuum), c is velocity of light in a vacuum, and ε is a dielectric constant of Ag (or a vacuum).[37,38] Importantly, along the long axis of a dimer, the ratio of the decay length of bulk Ag d_{Ag} to that of vacuum d_v remains constant ($d_{Ag}/d_v \sim 2.36$).[37,38] Thus, we can evaluate the accuracy in FDTD calculation through deviation of the ratio from ~2.36. Figure 8(d) shows the decay curves of the electric flux density at 418 nm with several mesh sizes. The ratios evaluated are 0.18, 0.4, and 2.0 with mesh size 0.98, 0.5, and 0.2 nm, respectively. The value of 2.0 is reasonably satisfactory to us considering that FDTD calculation using 0.2 nm mesh requires a computational time longer than 20 days. Indeed, the calculated electric flux density at the center of the gap is well consistent with self-consistent calculation of Fig. 2(b) in Ref. 32 as shown by the cross in Fig. 8(d).

Finally, we calculate the absolute SERRS cross-section spectra by the use of mesh size 0.2 nm to quantitatively evaluate SERRS-EM enhancement factors. In Fig. 9, we show a set of SERRS cross-section spectra acquired from the same dimer, with three different incident wavelengths of λ_L=532, 561, and 633 nm [Figs. 9(c)–9(e)]. The SERRS cross sections were calculated by multiplying $M_{EM}(\lambda_L, \lambda, \boldsymbol{r_o})$ and $\sigma_R(\lambda_L, \lambda)$ using three λ_L [Figs. 9(h)–9(j)],[4–7] where $\boldsymbol{r_o}$

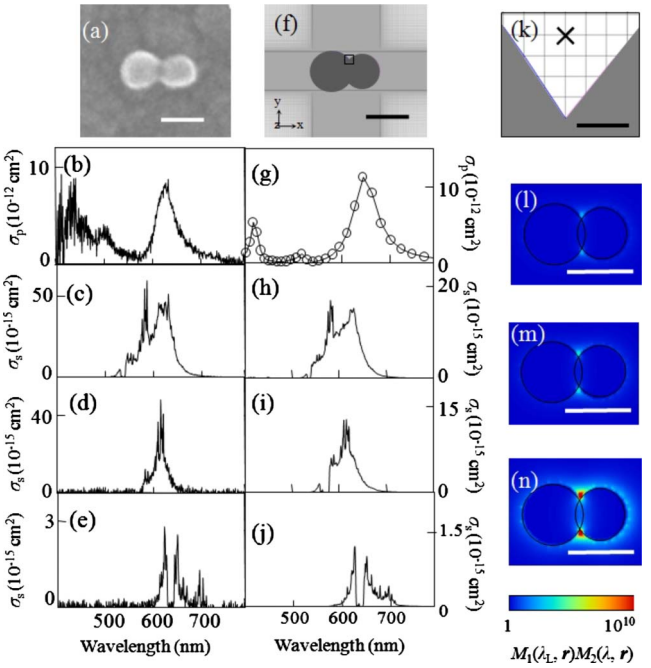

FIG. 9. (Color online) (a) SEM image of an Ag dimer, (b) experimental plasma-resonance spectrum, and experimental SERRS spectra excited at (c) 532, (d) 561, and (e) 633 nm. (f) Modeled structure of an Ag dimer in the FDTD calculation, (g) calculated plasma-resonance spectrum and calculated SERRS spectra excited at (h) 532, (i) 561, and (j) 633 nm. (k) Magnified view in the vicinity of the crevice of the model structure in (f). Spatial distribution of calculated SERRS-EM enhancement factor excited at (l) 532, (m) 561, and (j) 633 nm. Experimental plasma resonance maximum in (b) was ~620 nm, its FWHM was ~60 nm, and its cross section was $\sim 1\times 10^{-11}$ cm^2. Circularly polarized incident light (532, 561, and 633 nm), the mesh size 0.2 nm, and the refractive index 1.3 of the surrounding medium were selected in the FDTD calculation. Scale bars in (a), (f), (l)–(m) are 50 nm. Scale bar in (k) is 0.5 nm.

[the cross in Fig. 9(k)] is the location of the center of a R6G molecule. The center locates at ~0.8 nm from the Ag surface. The distance blocks charge-transfer interaction between R6G molecules and Ag surfaces.[39–41] The shape of the SERRS spectra is correctly reproduced in the calculations, and moreover, the experimental cross sections are consistent with the calculations within a factor of ~2. This value is acceptable considering the huge enhancement factor of 10^9 involved in the SERRS process. This quantitative consistency of the experimental SERRS spectra with the calculations for three incident wavelengths provide convincing evidence for the SERRS-EM theory, in which SERRS is described as the product of resonance Raman scattering and plasma resonance of the nanostructure.

IV. SUMMARY

We have studied the quantitative nature of the EM enhancement effect on SERRS, and demonstrated its absolute validity. Polarization-controlled observation of the plasma resonance and the SERRS spectra from single isolated Ag

nanostructures using dark-field microspectroscopy was combined with SEM observation to achieve one-to-one correspondence between optical anisotropy of plasma resonance, that of SERRS, and the morphology of the nanostructures. The experimental observations were compared with the calculations of the EM field based on individual morphology of the nanostructure. The enhancement factor of $\sim 10^9$ was correct within a factor of ~ 2 between the experiments and the calculations for three excitation wavelengths for SERRS. Our results fortify the indispensible importance of SERRS-EM theory to design metal nanostructures generating strong EM enhancement.

In the current study, Ag/Rhodamine was employed as the model system for SERRS EM enhancement. Here, the chemical enhancement effect was ignored. However, strong chemical enhancement is reported for Ag/Pyridine.[42,43] The chemical enhancement effect is most likely to depend on the specific target molecules; large molecules such as Rhodamine 6G, for which the resonance is hardly affected by adsorption, is probably reasonable to show diminished chemical effect. However, because the EM effect is less likely to be affected by chemical species, our current results on the quantitative nature of the EM effect should serve to separate the EM and the chemical effects, and to help quantify the degree of chemical enhancement in the near future.

ACKNOWLEDGMENTS

This work was supported by Scientific Research (Grant No. 19049013) on Priority Area "Strong Photons-Molecules Coupling Fields (470)," Grant-in-Aid for Scientific Research B (20510111), and C (21310071) from The Ministry of Education, Culture, Sports and Science and Technology (MEXT) of Japan, and in part by the Photon Frontier Network Program by MEXT.

*Corresponding author; tamitake-itou@aist.go.jp

[1] K. Kneipp, Y. Wang, H. Kneipp, L. T. Perelman, I. Itzkan, R. R. Dasari, and M. S. Feld, Phys. Rev. Lett. **78**, 1667 (1997).
[2] S. Nie and S. Emory, Science **275**, 1102 (1997).
[3] A. M. Michaels, M. Nirmal, and L. E. Brus, J. Am. Chem. Soc. **121**, 9932 (1999).
[4] H. Xu, E. J. Bjerneld, M. Käll, and L. Borjesson, Phys. Rev. Lett. **83**, 4357 (1999).
[5] H. Xu, X. H. Wang, M. P. Persson, H. Q. Xu, M. Käll, and P. Johansson, Phys. Rev. Lett. **93**, 243002 (2004).
[6] P. Johansson, H. Xu, and M. Käll, Phys. Rev. B **72**, 035427 (2005).
[7] M. Inoue and K. Ohtaka, J. Phys. Soc. Jpn. **52**, 3853 (1983).
[8] M. Moskovits, Rev. Mod. Phys. **57**, 783 (1985).
[9] B. Pettinger, J. Chem. Phys. **85**, 7442 (1986).
[10] We adopted the term "plasma resonance" in the current paper instead of well used term "plasmon resonance" to avoid the possible confusion because plasmon originally means a quantum of plasma oscillation inside metal and cannot couple with light.
[11] E. C. Le Ru and P. G. Etchegoin, Chem. Phys. Lett. **423**, 63 (2006).
[12] E. Le Ru, J. Grand, N. Félidj, J. Aubard, G. Lévi, A. Hohenau, J. Krenn, E. Blackie, and P. Etchegoin, J. Phys. Chem. C **112**, 8117 (2008).
[13] C. Orendorff, L. Gearheart, N. Jana, and C. Murphy, Phys. Chem. Chem. Phys. **8**, 165 (2006).
[14] K. Imura, H. Okamoto, M. Hossain, and M. Kitajima, Nano Lett. **6**, 2173 (2006).
[15] K. Imura, H. Okamoto, M. Hossain, and M. Kitajima, Chem. Lett. **35**, 78 (2006).
[16] H. Tamaru, H. Kuwata, H. Miyazaki, and K. Miyano, Appl. Phys. Lett. **80**, 1826 (2002).
[17] H. Kuwata, H. Tamaru, K. Esumi, and K. Miyano, Appl. Phys. Lett. **83**, 4625 (2003).
[18] J. Camden, J. Dieringer, Y. Wang, D. Masiello, L. Marks, G. Schatz, and R. Van Duyne, J. Am. Chem. Soc. **130**, 12616 (2008).
[19] T. Itoh, K. Hashimoto, and Y. Ozaki, Appl. Phys. Lett. **83**, 2274 (2003).
[20] T. Itoh, V. Biju, M. Ishikawa, Y. Kikkawa, K. Hashimoto, A. Ikehata, and Y. Ozaki, J. Chem. Phys. **124**, 134708 (2006).
[21] T. Itoh, K. Yoshida, V. Biju, Y. Kikkawa, M. Ishikawa, and Y. Ozaki, Phys. Rev. B **76**, 085405 (2007).
[22] K. Yoshida, T. Itoh, V. Biju, M. Ishikawa, and Y. Ozaki, Phys. Rev. B **79**, 085419 (2009).
[23] K. Yoshida, T. Itoh, V. Biju, M. Ishikawa, and Y. Ozaki, Proceedings of the 21st International Conference on Raman Spectroscopy (ICORS), 2008 (unpublished), p. 341.
[24] T. Itoh, H. Yoshikawa, K. Yoshida, V. Biju, and M. Ishikawa, J. Chem. Phys. **130**, 214706 (2009).
[25] A. Taflove and S. Hagness, *Computational Electrodynamics*, 3rd ed. (Artech house, Norwood, 2005).
[26] P. Lee and D. Misel, J. Phys. Chem. **86**, 3391 (1982).
[27] T. Itoh, T. Asahi, and H. Masuhara, Jpn. J. Appl. Phys. **41**, L76 (2002).
[28] T. Itoh, T. Uwada, T. Asahi, Y. Ozaki, and H. Masuhara, Can. J. Anal. Sci. Spectrosc. **52**, 130 (2007).
[29] K. Yoshida, T. Itoh, V. Biju, M. Ishikawa, and Y. Ozaki, Appl. Phys. Lett. **95**, 263104 (2009).
[30] C. Sönnichsen, S. Geier, N. Hecker, G. von Plessen, J. Feldmann, H. Ditlbacher, B. Lamprecht, J. Krenn, F. Aussenegg, V. Z.-H. Chan, J. P. Spatz, and M. Möller, Appl. Phys. Lett. **77**, 2949 (2000).
[31] D. S. Wang and M. Kerker, Phys. Rev. B **24**, 1777 (1981).
[32] H. Xu, J. Aizpurua, M. Käll, and P. Apell, Phys. Rev. E **62**, 4318 (2000).
[33] P. Matousek, M. Towrie, and A. Parker, J. Raman Spectrosc. **33**, 238 (2002).
[34] J. Alegret, T. Rindzevicius, T. Pakizeh, Y. Alaverdyan, L. Gunnarsson, and M. Käll, J. Phys. Chem. C **112**, 14313 (2008).
[35] T. Ambjörnsson, G. Mukhopadhyay, S. P. Apell, and M. Käll, Phys. Rev. B **73**, 085412 (2006).
[36] C. E. Talley, J. B. Jackson, C. Oubre, N. K. Grady, C. W. Hollars, S. M. Lane, T. R. Huser, P. Nordlander, and N. J. Halas,

Nano Lett. **5**, 1569 (2005).
[37] T. Ong, V. Celli, and A. Marvin, J. Opt. Soc. Am. A **11**, 759 (1994).
[38] See, for example, H. Reather, *Surface Plasmons on Smooth and Rough Surfaces and on Gratings* (Springer-Verlag, Berlin, 1988), Chap. 2.
[39] T. Sen, S. Sadhu, and A. Patra, Appl. Phys. Lett. **91**, 043104 (2007).
[40] T. Sen and A. Patra, J. Phys. Chem. C **112**, 3216 (2008).
[41] S. Saini, G. Srinivas, and B. Bagchi, J. Phys. Chem. B **113**, 1817 (2009).
[42] D. Wu, J. Li, B. Ren, and Z. Tian, Chem. Soc. Rev. **37**, 1025 (2008).
[43] A. Otto, Phys. Status Solidi A **188**, 1455 (2001).